SINAI International Scientific Journal (SISJ)
Volume 2, Issue 2, October 2025

Modeling and Control of CERT Microgrid

Ibrahim A. Awaad[1*], *Naema M. Mansour*[2], *Abdelazeem A. Abdelsalam*[2]

[1]*Department of Electrical, Faculty of Engineering, Sinai University- Arish Branch, Arish, Egypt.*
[2]*Electrical Engineering Dept., Faculty of Engineering, Suez Canal University, Ismailia, Egypt*
**Corresponding author*

Correspondence:

Ibrahim A. Awaad
ebrahim.abdallah@eng.suez.edu.eg

Citation:

Awaad, I. A. *Mansour*, N. M., and Abdelsalam, A. A., "Modeling and Performance Analysis of CERT Microgrid ", SINAI International Scientific Journal (SISJ), vol.2(2), pp. 21-36, 2025

Received: 11 August 2024

Accepted: 13 October 2024

ABSTRACT

The advancement of distributed energy resources (DER) technology provides doors for electricity customers to generate power on-site to meet the increasing demand for electricity from their customers. The microgrid developed by the Consortium for Electric Reliability Technology Solutions (CERTS) presents a unique method of using DER.Reliability, power quality, and operating costs can all be improved through MG integration. In a CERTS microgrid, this paper covers the modeling and analysis of several solar cells (PVs), battery storage, and a controlled load. A fault analysis study occurs and the operational features of the simulated CERTS microgrid are studied under various operating scenarios. An evaluation will be done on the modeling stability under various operating events. Additionally, the study provides a comprehensive examination of the MG structure and the associated control and protection challenges. The Matlab Simulink platform is used for modeling and various case studies.

Keywords: Microgrids, CERTS, photovoltaic cells, battery energy storage system, protection perspectives, energy management**..**

1. INTRODUCTION

The electrical power system gains a new dimension with the growing use of microgrids in electricity networks, and new challenges with the operation, control, and protection of electrical networks are created. A collection of interconnected DERs and loads that operate as a single, controllable unit within the grid is called a microgrid. It may work in grid-connected or island mode by connecting and disconnecting from the grid. However, microgrid connections enhance customer dependability and grid resilience [1-14]. Challenges that arise with microgrid communications include bi-directional power flow that strongly affects the coordination of the protection system, low fault current levels during islanding mode that require an improved intelligent protection system, and frequency control during islanding operation [15-22]. CERTS reviews the impact of these resources' widespread deployment and explores potential modifications to improve the reliability of the electrical grid.

The CERT microgrid concept assumes interconnecting a group of loads and DERs that must be power electronic based to offer the necessary flexibility to guarantee an isolated system's operation. Because of its control flexibility, the CERTS microgrid may interface with the bulk power system as a single controlled unit that satisfies regional security and reliability requirements. [23]. In contrast to traditional approaches for integrating DER, the CERTS microgrid introduced a well-controllable design to seamlessly isolate from the grid if the problems arise and reconnect once they are resolved. To fulfill these requirements, highly sensitive sensing units and high-speed switches are employed in the event of abnormal grid conditions to disconnect the microgrid from the electricity system. The DER units can meet essential load demands due to this technique and an advanced protection system and controller

Online ISSN: 3009-7800
Print ISSN: 3009-6324

to ensure power quality and reliability [24], [25]. The CERT microgrid concept is based on some basic requirements that are summarized as:

1. Ensuring load service continuity through automatic and easy transitions between grid-connected and islanded modes of operation.
2. Implement an advanced protection system compatible with low fault current.
3. Implementation of an advancing control system capable of maintaining voltage and frequency stability during islanding conditions without needing an advanced communication system.

A unique feature of the CERT microgrid concept is that sensitive communication systems are not required for the control of the separate DER units. When the switch operates, its controls automatically adjust to the new working conditions. In this paper, validation of the CERTS microgrid concept is introduced by introducing a comprehensive investigation into the design, optimization, and performance analysis of an integrated microgrid comprising multiple photovoltaic (PV) cells, battery energy storage system, and AC loads with embedded controllers. The microgrid stability is tested during different operating conditions such as grid-connected, islanding, and fault and loading conditions. Also, the control system of the microgrid is tested and evaluated during different operating conditions using the Matlab Simulink platform. A fault analysis study is carried out to reveal the operational challenges associated with microgrid connection from the protection perspective. The main work's key contributions may be summed up as follows:

- Modelling of the CERTS Microgrid Testbed System.
- Control of the CERTS Microgrid Testbed System.
- The stability of the model and the evaluation of the DER-controller during varying load values, variation of solar irradiance, and transition from grid-connected to islanding mode.
- The performance of the overcurrent scheme traditionally used in short-feeder protection.

In section II, the cert microgrid architecture and modeling are highlighted, simulation results are discussed in section III, and the conclusion is introduced in section IV.

2. CERTS MICROGRID SYSTEM ARCHITECTURE

According to the CERT microgrid concept, the microgrid structure assumes an aggregation of small sources and loads operating as an independent system providing electrical power. To achieve the required flexibility to ensure controlled operation as a single aggregated system, most of these sources are restricted to be power electronic-based to meet the local customers' needs related to reliability and security. Another important function of the control system is enabling the microgrid to operate in the grid-connected and islanding mode as well as a smooth transition between them [26-30]. An illustration of the CERT microgrid architecture is indicated in Fig. 1. The microgrid system is assumed to be a radial system with three feeders and a collection of loads. It includes two solar sources and one battery energy storage device, as well as four loads (L1, L2, L3, and L4) and three distributed energy resources. The DER-PV1, DER-PV2, and DER-Bt.s. Both inductive and capacitive loads are utilized. A step-down transformer is utilized to connect the CERTS microgrid system to the grid. Its ratings are 13.8 kV for the primary side and 0.480 kV for the secondary side [26, 32].

Online ISSN: 3009-7800
Print ISSN: 3009-6324

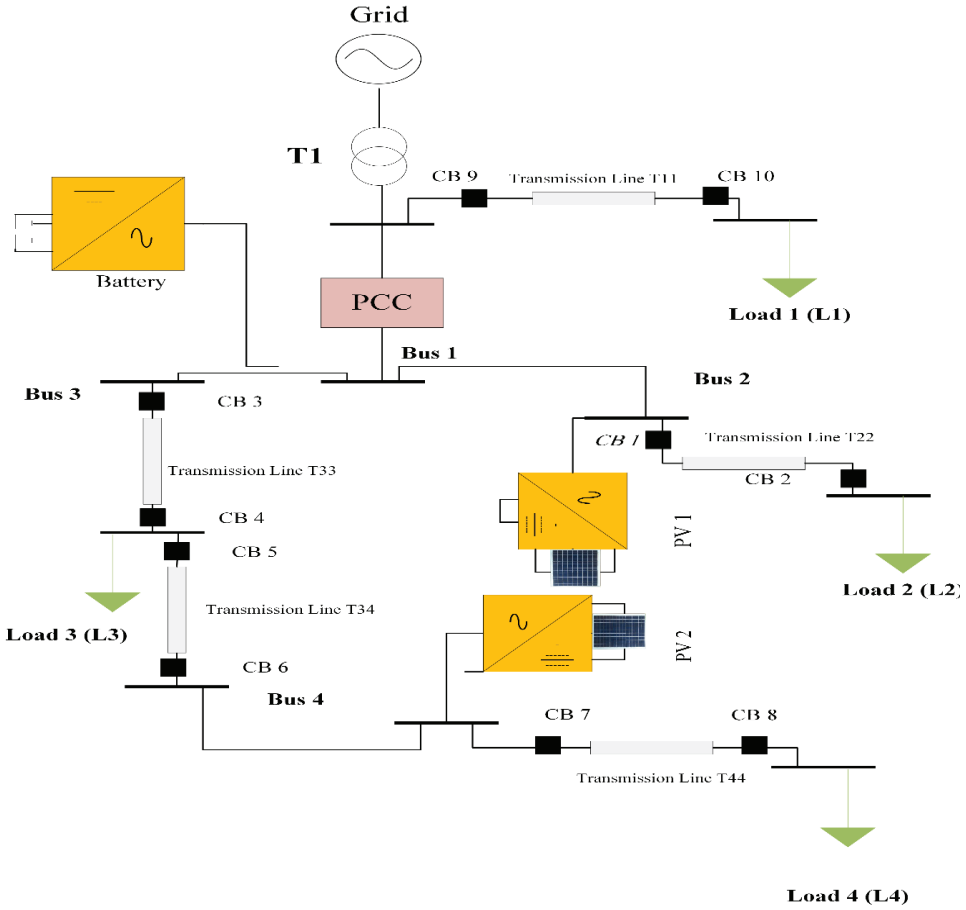

Fig. 1: CERTS Microgrid Architecture.

The four buses of the microgrid are connected via 5- feeders [T11, T22, T33, T34, T44], each feeder is 68.58. The parameters of the microgrid are indicated in Table 1. To create a well-controllable design CERTS microgrid that could seamlessly isolate from the grid, the three DER are interfaced to the grid using a voltage source converter (VSC) which is best suited to interconnecting a microgrid to the main power grid.

Table 1: Parameters of the CERTS microgrid system.

Parameter	Value
T1	15.0 MVA, 60Hz, 13.8/0.48KV, X/R=6, Z=5%
L3, L4	90KW,45KVAR
L5	90KW, -40KVAR
L6	90KW, -20KVAR
Load parameter	Value
Line11, Line22, Line33, and Line 44	Size (AWG2),68.58m, 60Hz
Line34	Size (AWG2/0),22.86m
DER-PV1, DER-PV2	200KW, Unity Power Factor (3-Phase Capacitor Bank (15kVA)).

Online ISSN: 3009-7800
Print ISSN: 3009-6324

By its capability to fast reactive power flow and voltage control at its terminals, VSC could enable a black start to energize connected microgrid or re-energizing grid; contributing to power system and voltage stability. Three different control methodologies were used to ensure the seamless transitions between grid-connected and islanded modes of the microgrid. battery energy storage combines a current-mode control in the d-q frame with an active/reactive power controller [33]. to ensure that the solar array produces the maximum amount of electricity, modified-current mode control with DC link voltage is the control methodology used for PV1 in disconnected mode only and for PV2 in both connected to the grid and islanding mode. Frequency-mode control is utilized to regulate the voltage and frequency of PV1 when it is in the islanding mode. Three distinct control approaches were applied for VSC:

2.1. VSC- Current-Mode Control

The VSC-current mode controller is used to manage and control the microgrid sources' three-phase active and reactive power during grid-connected mode. The three-phase quantities transform into a rotating d-q frame using park transformation, which reduces the number of control loops from three to two and makes controller design and simulation easier. The phase shift and amplitude of the line current are adjusted to regulate the power and reactive power. The foundation of the transformation and controller is described by the following equations [34].

$$\begin{matrix} \sin(\theta) & \sin\left(\theta-\frac{2\pi}{3}\right) & \sin\left(\theta+\frac{2\pi}{3}\right) \\ \cos(\theta) & \cos\left(\theta-\frac{2\pi}{3}\right) & \cos\left(\theta+\frac{2\pi}{3}\right) \\ \frac{1}{2} & \frac{1}{2} & \frac{1}{2} \end{matrix} \begin{bmatrix} V_{sa} \\ V_{sb} \\ V_{sc} \end{bmatrix} \quad (1)$$

$$P_s(t) = \frac{3}{2}\left(v_{sd}(t)\, i_{sd}(t) + v_{sq}(t)\, i_{sq}(t)\right) \quad (2)$$

$$Q_s(t) = \frac{3}{2}\left(-v_{sd}(t)\, i_{sq}(t) + v_{sq}(t)\, i_{sd}(t)\right) \quad (3)$$

Fig. 2 shows a schematic design of a current-controlled VSC system. In this controller mode, the control signals $X_{sd}(t)$, $v_{sq}(t)$, $i_d(t)$, and $i_q(t)$, respectively, are produced by transferring the grid voltages and three-phase VSC output currents from the abc-to-dq0 frame. A compensator processes these data to create the VSC's modulation or control signals [34]. To match the VSC currents with the grid voltage, it is required to determine the grid voltage's phase angle. Phase-locked loop (PLL) synchronization is used in this concept to rapidly track grid phasing irregularities. The PLL component generates the synchronization angle to reduce steady-state errors, simplify the compensator design, make system control easier, and maintain the $v_{sq}(t)$ constant at zero in the steady-state situation [35]. The following equations must be fulfilled to produce the reference current values in the d-q frame (i_{dref}), (i_f), and to match the required values with the real and reactive power supplied by the system:

$$i_{dref}(t) = \frac{2}{3v_{sd}}\left(P_{sref}(t)\right) \quad (4)$$

Online ISSN: 3009-7800
Print ISSN: 3009-6324

$$i_{qref}(t) = \frac{2}{3v_{sd}}\left(Q_{\text{sref}}(t)\right) \tag{5}$$

Subsequently, the AC side voltages and currents are created and fed into the compensator together with the reference currents. converted the compensator's output from the dq0 frame back to three phases, which were then sent into the PWM generator to produce the gating signals required for the VSC to fire [36].

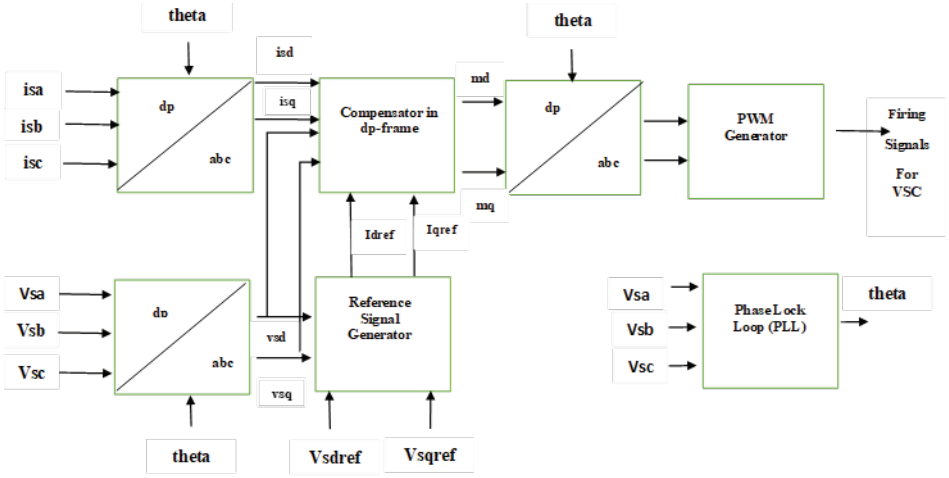

Fig. 2: Schematic diagram of a current-controlled VSC.

2.2. Controlled-Frequency VSC System

The voltage and frequency at the point of common coupling (PCC), which regulates the active and reactive power that the VSC system exchanges with the AC system, are regulated by the islanding mode in a controlled-frequency VSC system. During grid disturbance conditions, the microgrid should be isolated and operate in stand-alone mode then, is required to maintain typical frequency values on all buses and the voltage values as well. PV1 operates in both islanded and grid-connected modes, hence frequency mode control mechanism is employed when it is in islanding mode. The solar source-1 PV1's frequency control model implementation is shown in Fig. 3 [35-37].

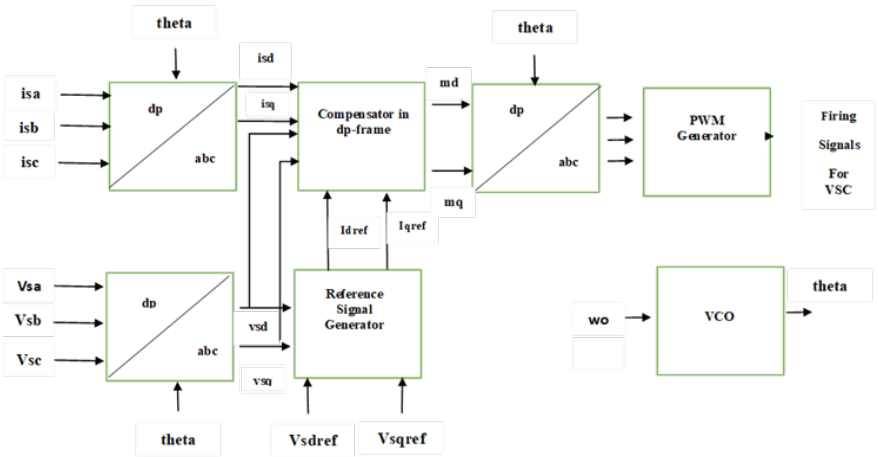

Fig. 3: Modelling of the frequency controller for the PV1.

Online ISSN: 3009-7800
Print ISSN: 3009-6324

2.3. Modified Current-Mode Control with DC Link Voltage

In [36-45], the VSC current-mode control principles are discussed in detail. The enhancement in this controller is concerned with regulating of power factor of the PV system. Controlling the power generated by the PV system is achieved by controlling the DC link voltage. the goal of the DC link voltage-control method is to guarantee stable PV behavior and the safe operation of the VSC. Fig. 4 shows the updated current mode with DC link voltage control implemented.

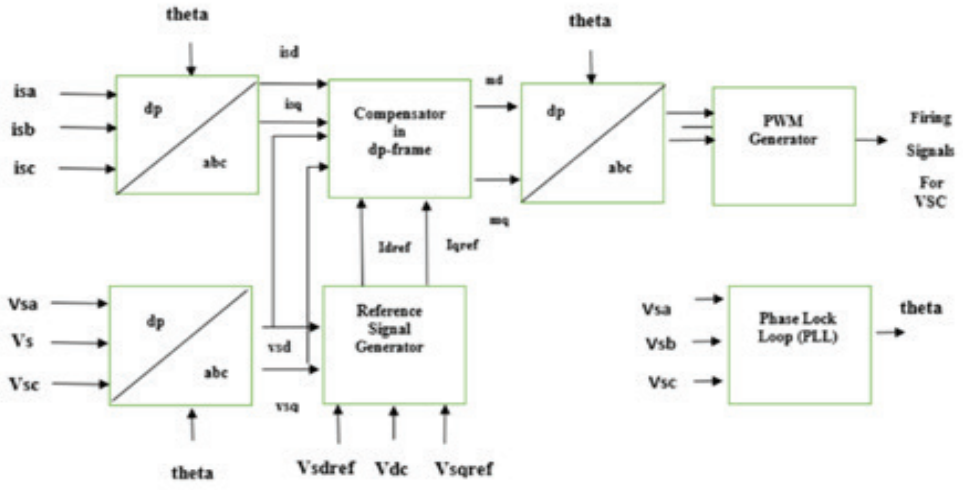

Fig. 4: Modified current-mode controls with DC link voltage schematic diagram.

3. SIMULATION RESULTS AND DISCUSSIONS

In this section, the MATLAB Simulink platform was used to perform tests and evaluate the simulated CERTS microgrid system under various operational situations. In islanding and grid-connected modes, the produced voltage, currents, and power are analyzed under various load conditions to assess the grid stability. A fault analysis investigation helps to better understand the challenges associated with traditional protection techniques in microgrids. Also, the dynamic performance of the CERT microgrid system model appears under various loading cases, including normal loading conditions, changing from grid-connected to islanding mode, unexpected loading fluctuations, varying solar irradiation levels, and system initialization from reset (zero initial conditions). At each of the microgrid's four main buses (Bus1, Bus2, Bus3, Bus4), the voltage and current signals are recorded (see Fig. 1).

3.1. Normal Loading Condition

In the grid-connected mode, the microgrid is started at rest with zero initial conditions and its full load. The modeled system can be noticed achieving its steady-state values in 0.25 seconds (Fig. 5 (a) & (b)). Additionally, as shown in (Fig. 8 (a) & (b)), the microgrid system achieved its steady-state values during islanding mode in 0.25 seconds. It takes roughly 0.25 seconds for the waveforms of voltage and current to adjust to their steady-state levels. the output of pv1 and pv2 are shown in (Fig. 6, Fig.7, Fig. 9, Fig. 10) while operating in islanding and connected modes.

Online ISSN: 3009-7800
Print ISSN: 3009-6324

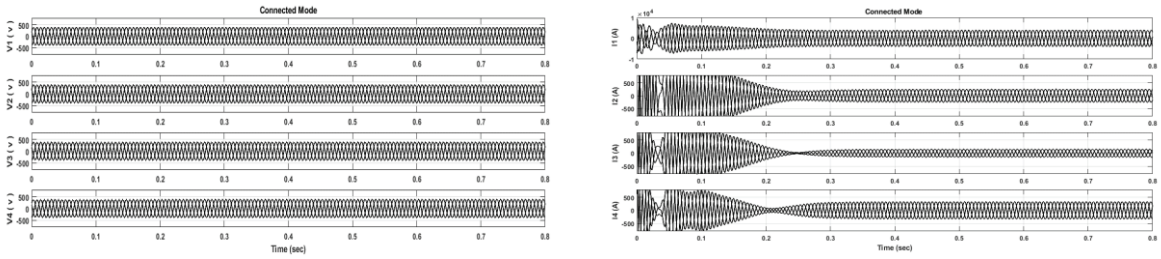

(a) Voltage waveforms. (b) Current waveforms

Fig. 5: Voltage and current waveforms of the micro-grid system measured at Bus1-Bus 4 during initialization of the grid-connected condition.

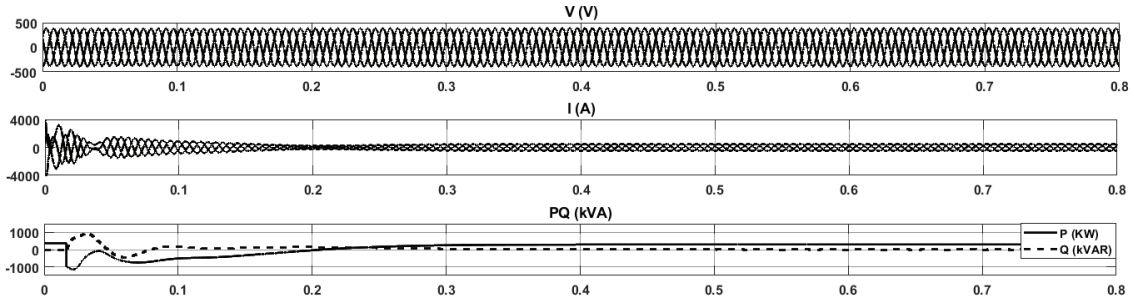

Fig. 6: Voltage, current, and power waveforms of the micro-grid system measured at PV1 during initialization of the grid-connected condition.

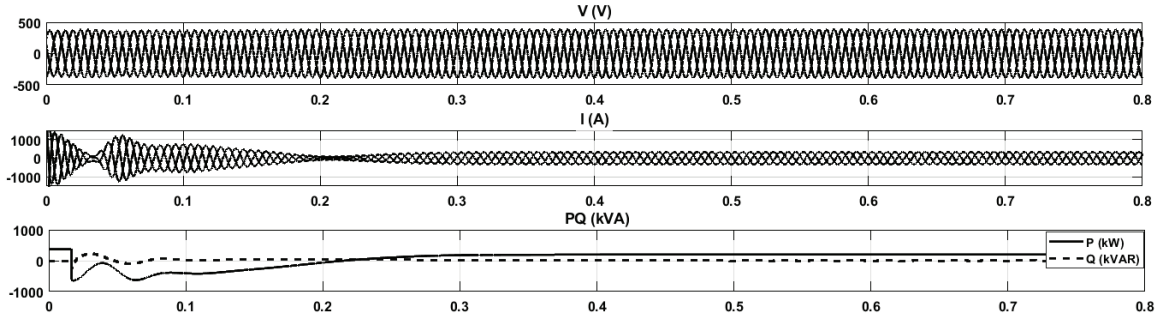

Fig. 7: Voltage, current, and power waveforms of the micro-grid system measured at PV2 during initialization of the grid-connected condition.

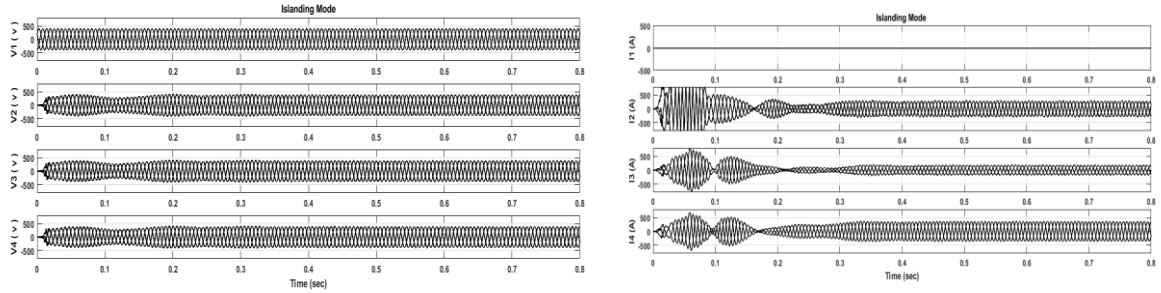

(a) Voltage waveforms. (b) Current waveforms

Fig. 8: Voltage and current waveforms of the micro-grid system measured at Bus1-Bus 4 during initialization of the islanding mode condition.

Online ISSN: 3009-7800
Print ISSN: 3009-6324

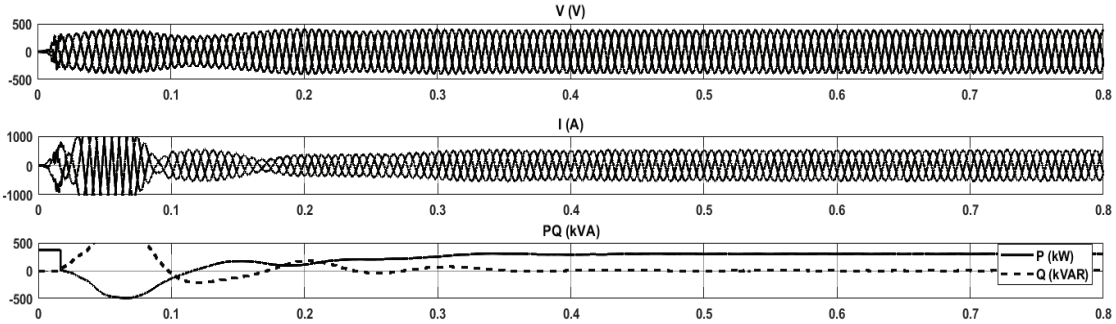

Fig. 9: Voltage, current, and power waveforms of the micro-grid system measured at PV1 during initialization of the islanding-connected condition.

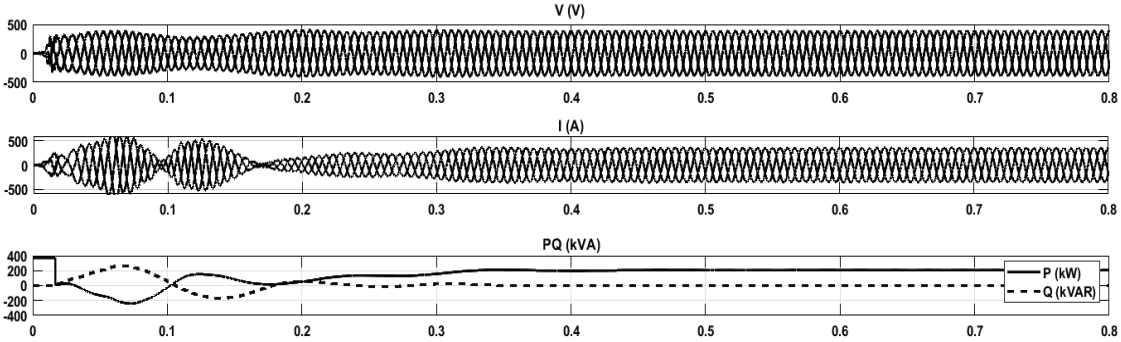

Fig. 10: Voltage, current, and power waveforms of the micro-grid system measured at PV2 during initialization of the islanding-connected condition.

3.2. Transition from Grid-Connected to Islanding Mode

The transition from grid-connected to islanding mode involves significant changes in voltage and current due to the disconnection from the main grid. the transition from grid-connected to islanding mode involves careful detection, control, and stabilization processes. effective management is crucial to ensure voltage and current levels remain stable, safeguarding the reliability of the local power system. The stability of the modeled CERT microgrid system is tested during the transition from grid-connected mode to islanding mode. As shown in Fig. 11, if the microgrid is disconnected from the main grid after 0.7sec, it can restore its steady state within 0.8sec. The voltage waveforms are exposed to a slight change in their magnitudes at the instant of isolation, but they quickly regain their steady-state values within 0.8sec as shown in Fig. 11 (a). Also, the current waveforms were rabidly increased at the moment of isolation, but they regained their steady values within 0.8 sec, as in Fig. 11 (b).

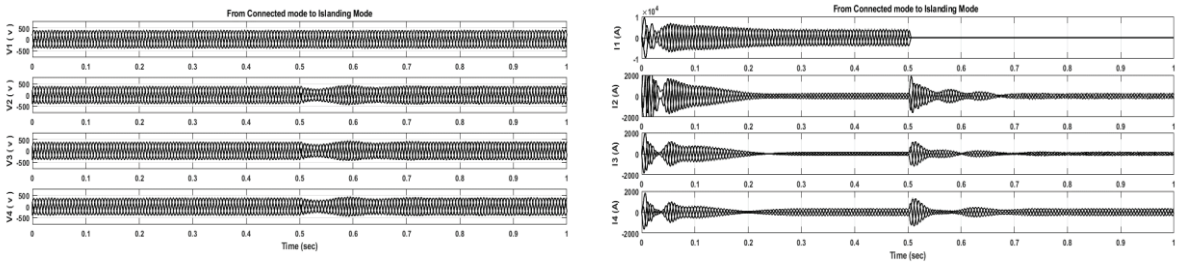

(a) Voltage waveforms. **(b) Current waveforms**

Fig. 11: Voltage and current waveforms of the micro-grid system measured at Bus1-Bus 4 during the transition from grid-connected mode to islanding mode.

Online ISSN: 3009-7800
Print ISSN: 3009-6324

3.3. Sudden Change in Loading Values

Sudden changes in load magnitude have significant implications for grid stability in both grid-connected and islanding modes. in grid-connected mode, the external grid can provide support, mitigating some impacts, whereas, in islanding mode, the isolation increases sensitivity to voltage and frequency instability. effective management strategies are essential in both scenarios to maintain stability and reliability.in islanding mode, an increase in load can lead to more severe voltage drops since the grid has no external support as shown in Figs. 13 and 14. In grid-connected mode, if the additional load is added in parallel with load 3 (L3) at 0.8 sec, the voltage waveforms could keep their stable values as in Fig. 12 (a), and the electrical current drawn from the grid increased, and this appeared to increase in Bus 1 and Bus 3 currents as in Fig. 12 (b). In contrast, the voltage magnitude shows a reasonable decrease at the moment of load change during islanding mode as in Fig. 13 (a), and the current magnitude of the current measured at all the microgrid buses is increased as in Fig. 13 (b). The CERT microgrid system could maintain its stability during load change.

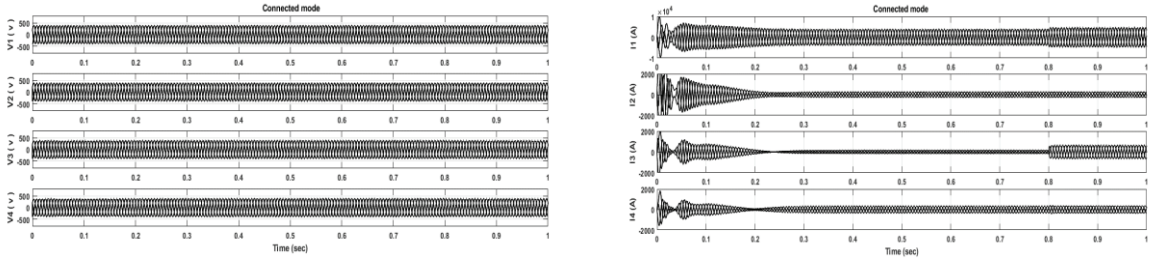

(a) Voltage waveforms. (b) Current waveforms

Fig. 12: Voltage and current waveforms of the micro-grid system measured at Bus1-Bus 4 for the sudden change in load magnitude during the grid-connected mode.

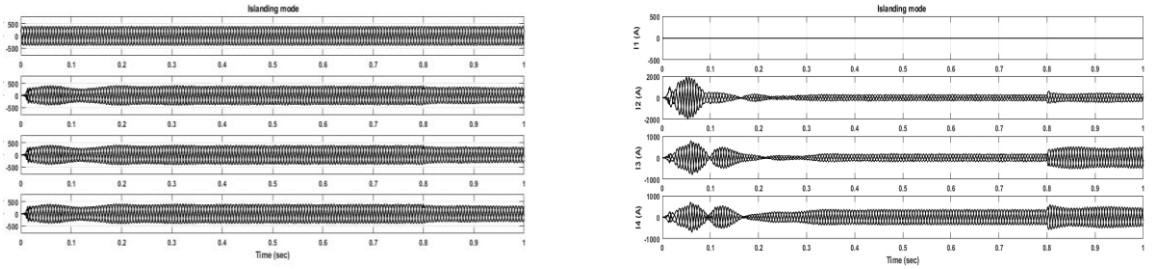

(a) Voltage waveforms. (b) Current waveforms

Fig. 13: Voltage and current waveforms of the micro-grid system measured at Bus1-Bus 4 during a sudden change in load magnitude in islanding mode.

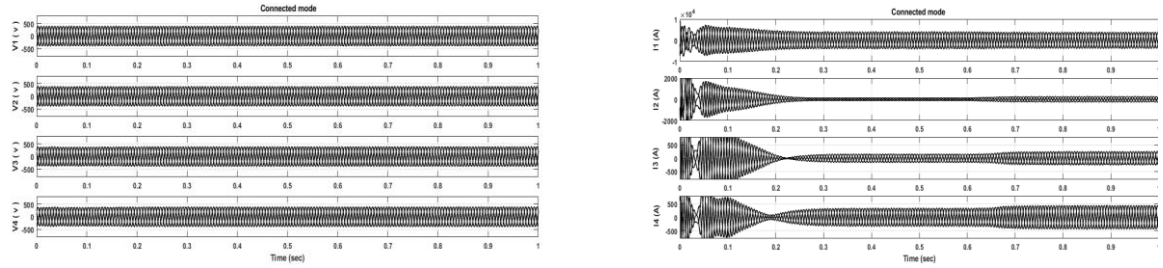

(a) Voltage waveforms. (b) Current waveforms

Fig. 14: Voltage and current waveforms of the micro-grid system measured at Bus1-Bus 4 for the sudden change in solar irradiance magnitude at 0.5sec during the grid-connected mode.

Online ISSN: 3009-7800
Print ISSN: 3009-6324

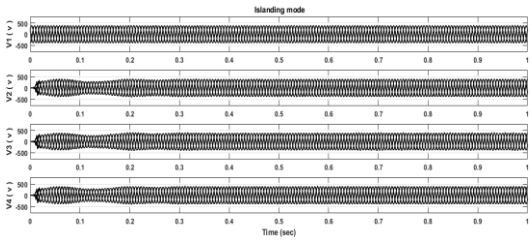

(a) Voltage waveforms.

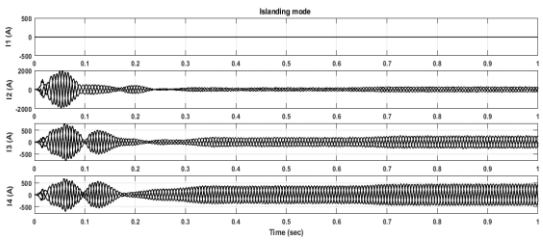

(b) Current waveforms

Fig. 15: Voltage and current waveforms of the micro-grid system measured at Bus1-Bus 4 for the sudden change in solar irradiance magnitude at 0.5sec during the grid-connected mode.

3.4. Change of Solar Irradiance

The solar irradiance variation effects on the response of the CERT microgrid system during grid-connected and islanding modes are indicated in Fig. 14 and 15. The irradiation value is increased from 600 w/m2 to 800 w/m2 at 0.6 sec, the CERT microgrid system is responding to this increase by the current magnitude increasing.

3.5. Fault Analysis Study

The three-phase short circuit at the mid-point of the feeder T22 during the grid-connected and islanding modes is carried out, and the voltage and current magnitudes are recorded as in Figs. 16 and 17. It can be noticed that the steady-state fault current level recorded at Bus 4 for grid-connected mode is greater than that for islanding mode due to the fault current support from the grid. In the grid-connected mode, the fault current level could be easily detected by the traditional overcurrent protection scheme, and the fault could be successfully isolated.

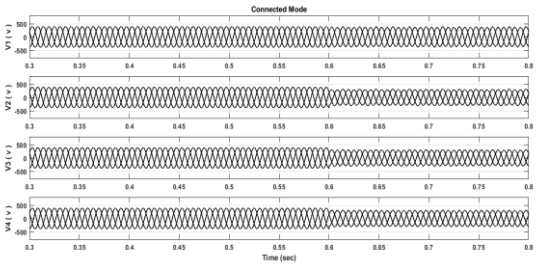

(a) Voltage waveforms.

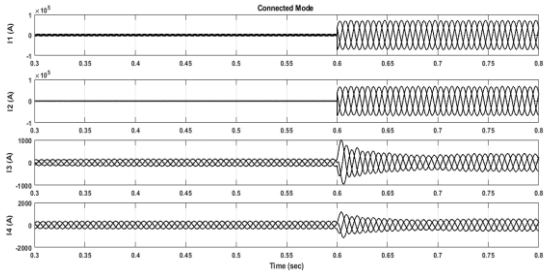

(b) Current waveforms

Fig. 16: Voltage and current waveforms of the micro-grid system measured at Bus1-Bus 4 for solidly ABC fault at the mid-point of feeder T22 during grid-connected mode.

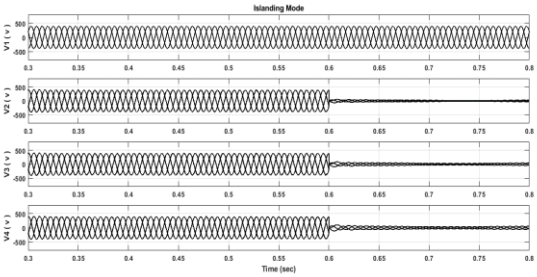

(a) Voltage waveforms.

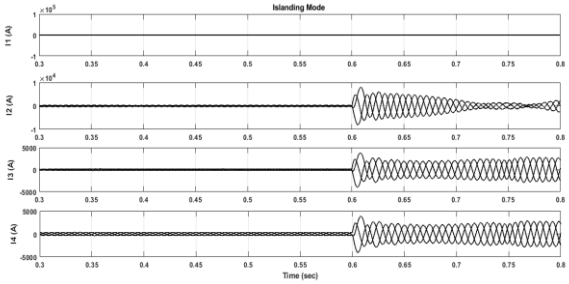

(b) Current waveforms

Fig. 17: Voltage and current waveforms of the micro-grid system measured at Bus1-Bus 4 for solidly ABC fault at the mid-point of feeder T22 during the islanding mode.

Online ISSN: 3009-7800
Print ISSN: 3009-6324

In grid mode, Protective relays detect the fault quickly. they measure current and voltage levels and identify abnormal conditions. once detected, breakers isolate the faulted section from the rest of the grid. all phase voltages drop to near zero at the fault location, but the rest of the grid can maintain voltage levels due to the support from other generation sources. fault currents surge significantly, often many times the normal current levels as shown in Fig. 16. In islanding mode, the system may lack effective detection mechanisms for faults. local protective devices may not function as they would in grid-connected mode. all phase voltages drop significantly at the fault location, and there is no external support to stabilize them. the overall voltage may collapse. fault currents surge significantly but the current value is not as big as grid mode as shown in Fig. 17. In contrast, the steady-state fault current level during island mode that is recorded at Bus 2 (I2) is decreased, and its magnitude may not be detected by the traditional overcurrent relay scheme. However, the three-phase fault in both grid-connected and islanding modes could be successfully detected; the situation will be worse if the fault resistance is considered, especially in islanding mode. Fig. 16 shows that despite a three-phase fault at Bus 2, which is close to the point of common coupling (PCC), the grid support prevents a significant reduction in voltage. On the other hand, because of its distance from the grid, the voltage decreases for the identical fault at line T44's midpoint is noteworthy; see Fig. 18, the voltage magnitude at Bus 4 (V4). The fault current magnitudes recorded for the islanding mode are large and the fault could be isolated with the traditional protection schemes, see Fig. 19.

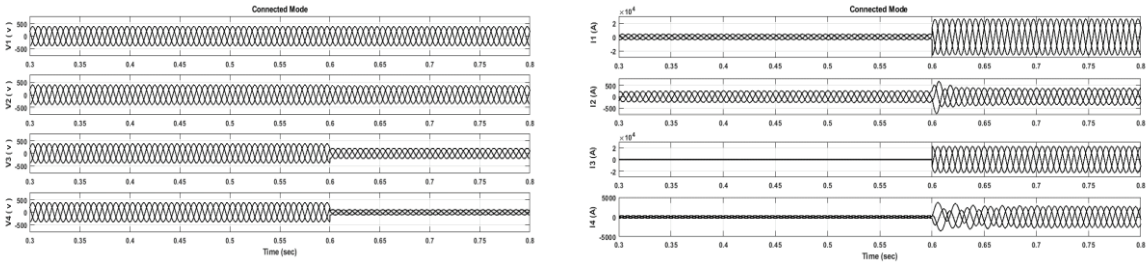

(a) Voltage waveforms. **(b) Current waveforms**

Fig. 18: Voltage and current waveforms of the micro-grid system were measured at Bus1-Bus 4 for solidly ABC fault at the mid-point of feeder T44 during the grid-connected mode.

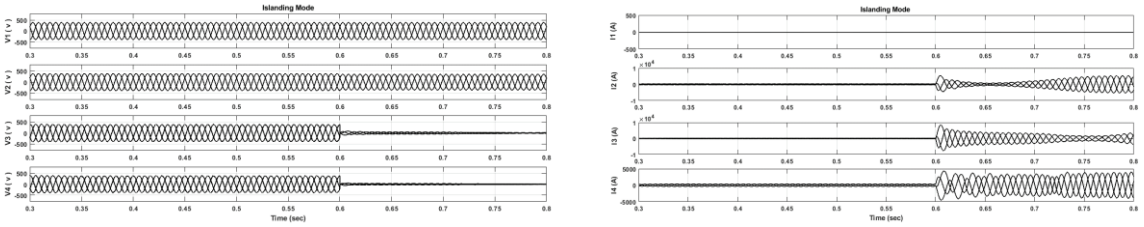

(a) Voltage waveforms. **(b) Current waveforms**

Fig. 19: Voltage and current waveforms of the micro-grid system were measured at Bus1-Bus 4 for solidly ABC fault at the mid-point of feeder T44 during the grid-connected mode.

Traditionally, the short feeders are usually protected by a simple overcurrent protection scheme that is initiated by the fault current magnitude. If the fault resistance is considered, the traditional protection scheme will not be sufficient for a microgrid system in islanding mode. The same responses for solidly AB fault at the midpoint of feeder T44 are achieved, the fault

Online ISSN: 3009-7800
Print ISSN: 3009-6324

current level is decreased in the islanding mode than grid-connected mode as in Figs. 20 and 21.

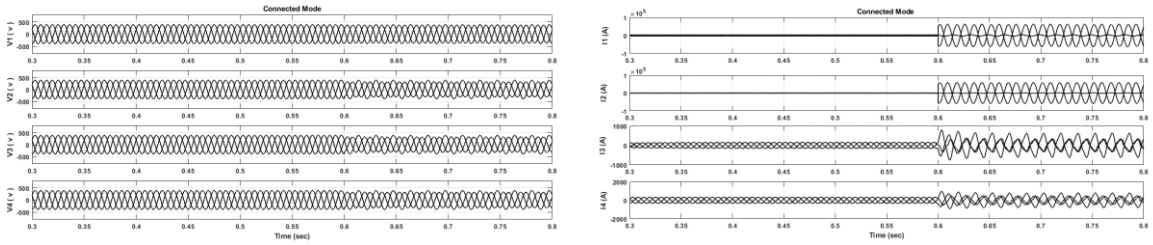

(a) Voltage waveforms. **(b) Current waveforms**

Fig. 20: Voltage and current waveforms of the micro-grid system measured at Bus1-Bus 4 for solidly AB fault at the mid-point of feeder T22 during grid-connected mode.

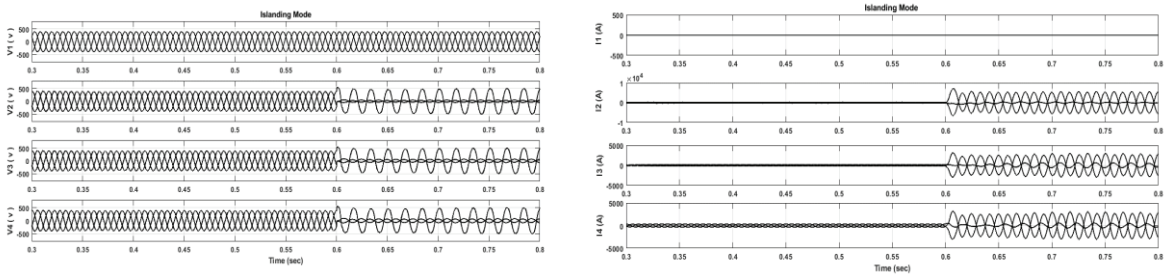

(a) Voltage waveforms. **(b) Current waveforms**

Fig. 21: Voltage and current waveforms of the micro-grid system measured at Bus1-Bus 4 for solidly AB fault at the mid-point of feeder T22 during islanding mode.

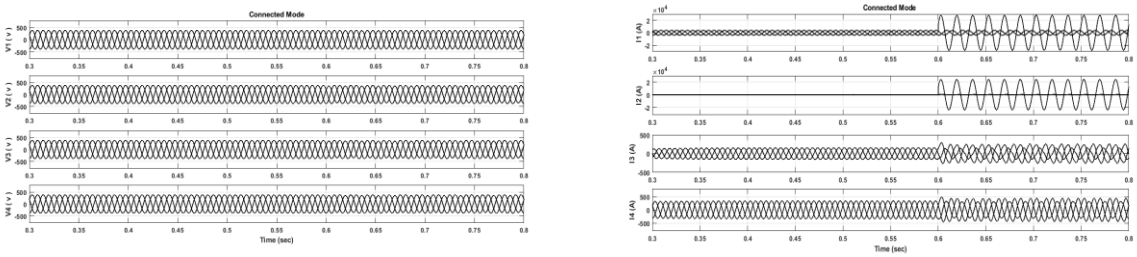

(a) Voltage waveforms. **(b) Current waveforms**

Fig. 22: Voltage and current waveforms of the micro-grid system measured at Bus1-Bus 4 for solidly AG fault at the mid-point of feeder T22 during grid-connected mode.

The larger grid can provide support, maintaining voltage levels despite the fault. The faulted phase may drop in voltage depending on the distance bus from the grid, but other phases may remain stable as shown in Fig. 22. the fault causes a significant voltage drop in the affected phase, leading to an imbalance in the system voltages (e.g., phase A may see a large reduction in voltage while phases B and C remain higher) as shown in Fig. 23. The grid's vast capacity helps limit the fault current. Protective relays can quickly detect the fault and isolate the affected section, minimizing the impact. The fault current in grid mode is higher than islanding mode due to the grid contributes in fault current as in Fig. 22 (b) and Fig. 23 (b). The situation is worsened for phase-to-ground faults; an AG fault occurs at the midpoint of feeder T22; the voltage magnitude in the case of grid-connected is slightly affected; and the fault current contribution from the grid is high and can be detected as shown in Fig. 22. In contrast, the fault

Online ISSN: 3009-7800
Print ISSN: 3009-6324

current contribution from the DERs during islanding mode is insufficient to be detected by the traditional protection elements, as shown in Fig. 23. Also, there is a sensible overvoltage in the healthy phases in the islanding mode.

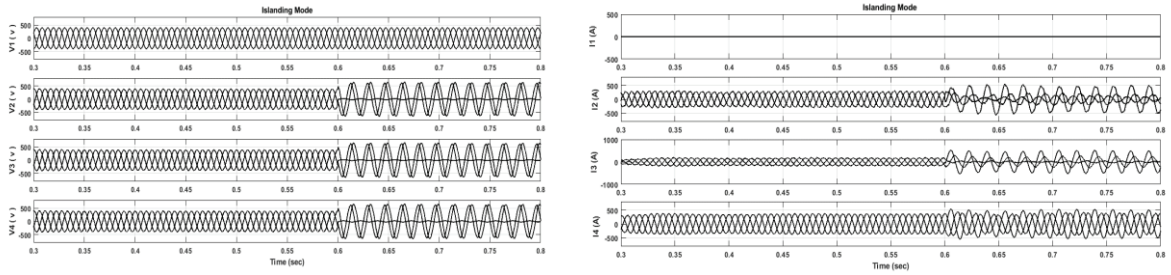

(a) Voltage waveforms. **(b) Current waveforms**

Fig. 23: Voltage and current waveforms of the micro-grid system measured at Bus1-Bus 4 for solidly AG fault at the mid-point of feeder T22 during the islanding mode.

4. CONCLUSIONS

In this paper, an effective model of the CERTS microgrid testbed system is introduced. The model is tested in both grid-connected and islanding modes for different normal and abnormal conditions. The stability of the model and the evaluation of the DER-controller during varying load values, variation of solar irradiance, and transition from grid-connected to islanding mode. The introduced model is used to evaluate the performance of the overcurrent scheme traditionally used in short feeder protection. A detailed fault analysis study is carried out through the modeling of different fault types at different locations during the grid-connected and islanding modes. The study concluded that the traditional protection scheme based on overcurrent relays was unable to provide efficient protection for microgrids during the islanding mode. So, the smart protection scheme is required for perfect fault detection, classification, and isolation of microgrids during islanding mode.

CONFLICT OF INTEREST

The authors declare no conflict of interest.

FUNDING

No funding.

REFERENCES

[1] Barra, P., Coury, D., & Fernandes, R. (2020). A survey on adaptive protection of microgrids and distribution systems with distributed generators. Renewable and Sustainable Energy Reviews, 118, 109524. https://doi.org/ 10.1016/j.rser.2019.109524.

[2] Alasali, Feras, et al. "Powering up microgrids: A comprehensive review of innovative and intelligent protection approaches for enhanced reliability." Energy Reports 10 (2023): 1899-1924.

[3] Khubrani, Mousa Mohammed, and Shadab Alam. "Blockchain-based microgrid for safe and reliable power generation and distribution: a case study of Saudi Arabia." Energies 16.16 (2023): 5963.

Online ISSN: 3009-7800
Print ISSN: 3009-6324

[4] Khare, Vikas, and Pradyumn Chaturvedi. "Design, control, reliability, economic and energy management of microgrid: A review." e-Prime-Advances in Electrical Engineering, Electronics and Energy (2023): 100239.
[5] Lei B, Ren Y, Luan H, Dong R, Wang X, Liao J, Fang S, Gao K. A review of optimization for system reliability of microgrid. Mathematics. 2023 Feb 6;11(4):822.
[6] Alshehri, Mohammed Abdullah H., Youguang Guo, and Gang Lei. "Energy Management Strategies of Grid-Connected Microgrids under Different Reliability Conditions." Energies 16.9 (2023): 3951.
[7] Olivares DE, Mehrizi-Sani A, Etemadi AH, Cañizares CA, Iravani R, Kazerani M, Hajimiragha AH, Gomis-Bellmunt O, Saeedifard M, Palma-Behnke R, Jiménez-Estévez GA. Trends in microgrid control. IEEE Transactions on smart grid. 2014 May 20;5(4):1905-19.
[8] Lasseter RH. "MicroGrids," in Proc. IEEE Power Eng. Soc. Winter Meeting, Jan. 2002, vol. 1, pp. 305–308.
[9] Gopalan, S., Sreeram, V., & Iu, H. (2014). A review of coordination strategies and protection schemes for microgrids. Renewable and Sustainable Energy Reviews, 32, 222–228. doi.org/10.1016/j.rser.2014.01.037,
[10] Sedhom, B., El-Saadawi, M., El Moursi, M., Hassan, M., & Eladl, A. IoT-based optimal demand side management and control scheme for smart microgrid. International Journal of Electrical Power & Energy Systems, 127, 106674. (2021). doi.org/10.1016/j.ijepes.2020.106674
[11] Shahgholian G. A brief review on microgrids: Operation, applications, modeling, and control. International Transactions on Electrical Energy Systems. 2021 Jun;31(6):e12885.
[12] Hu J, Zhang T, Du S, Zhao Y. An overview on analysis and control of micro-grid system. International Journal of Control and Automation. 2015 May;8(6):65-76.
[13] Singh, I. Elamvazuthi, P. Nallagownden, G. Ramasamy, A. Jangra, Routing-based multi-agent system for network reliability in the smart microgrid, Sensors 20 (10) (2020) 2992.
[14] Y. Yoldaş, A. Önen, S. M. Muyeen, A. v. Vasilakos, and İ. Alan, 'Enhancing smart grid with microgrids: Challenges and opportunities, Renewable and Sustainable Energy Reviews, vol. 72. Elsevier Ltd, pp. 205–214, 2017. Doi: 10.1016/j.rser.2017.01.064.
[15] X. Kang, C. E. K. Nuworklo, B. S. Tekpeti, and M. Kheshti, 'Protection of micro-grid systems: a comprehensive survey, The Journal of Engineering, vol. 2017, no. 13, pp. 1515–1518, Jan. 2017, Doi: 10.1049/joe.2017.0584.
[16] IEEE Staff and IEEE Staff, 2012 IEEE Power and Energy Society General Meeting.
[17] P. Basak, S. Chowdhury, S. Halder Nee Dey, and S. P. Chowdhury, 'A literature review on integration of distributed energy resources in the perspective of control, protection, and stability of microgrid', Renewable and Sustainable Energy Reviews, vol. 16, no. 8. pp. 5545–5556, Oct. 2012. Doi: 10.1016/j.rser.2012.05.043.
[18] Sepehrirad I, Ebrahimi R, Alibeiki E, Ranjbar S. Intelligent differential protection scheme for controlled islanding of microgrids based on decision tree technique. Journal of Control, Automation and Electrical Systems. 2020 Oct;31(5):1233-50.
[19] Mohamad, Hasmaini, Hazlie Mokhlis, and Hew Wooi Ping. "A review on islanding operation and control for distribution network connected with small hydropower plant." Renewable and Sustainable Energy Reviews 15.8 (2011): 3952-3962.
[20] Isazadeh, Ghader, Amin Khodabakhshian, and Eskandar Gholipour. "New intelligent controlled islanding scheme in large interconnected power systems." IET Generation, Transmission & Distribution 9.16 (2015): 2686-2696.
[21] Koohi-Kamali, Sam, and Nasrudin Abd Rahim. "Coordinated control of smart microgrid

Online ISSN: 3009-7800
Print ISSN: 3009-6324

during and after islanding operation to prevent under frequency load shedding using the energy storage system." Energy conversion and management 127 (2016): 623-646.

[22] Baghaee, Hamid Reza, et al. "Anti-islanding protection of PV-based microgrids consisting of PHEVs using SVMs." IEEE Transactions on Smart Grid 11.1 (2019): 483-500.

[23] R. Lasseter, A. Akhil, C. Marnay, J. Stephens, J. Dagle, R. Guttromsom, A. S. Meliopoulous, R. Yinger, and J. Eto, "Integration of distributed energy resources - The CERTS microgrid concept," Lawrence Berkeley National Lab. (LBNL), Berkeley, CA (United States), Tech. Rep., 2002.

[24] D. K. Nichols, J. Stevens, R. H. Lasseter, J. H. Eto, and H. T. Vollkommer, "Validation of the CERTS microgrid concept the CEC/CERTS microgrid testbed," 2006 IEEE Power Engineering Society General Meeting, Montreal, QC, Canada, 2006, pp. 3 pp. doi: 10.1109/PES.2006.1709248.

[25] Eto J, Lasseter R, Schenkman B, Stevens J, Klapp D, VolkommeRr H, Linton E, Hurtado H, Roy J. Overview of the CERTS microgrid laboratory test bed. In2009 CIGRE/IEEE PES Joint Symposium Integration of Wide-Scale Renewable Resources Into the Power Delivery System 2009 Jul 29 (pp. 1-1).

[26] Ranjit, Ajit A., Mahesh S. Illindala, and Abrez Mondal. "CERTS microgrid: Modeling analysis and control of distributed energy resources—Phase I." Lawrence Berkeley National Laboratory, Berkeley, CA, USA (2015).

[27] Ranjit, Ajit A., Mahesh S. Illindala, and David A. Klapp. "Modeling and analysis of the CERTS microgrid with natural gas-powered distributed energy resources." 2015 IEEE/IAS 51st Industrial & Commercial Power Systems Technical Conference (I&CPS). IEEE, 2015.

[28] Alegria, Eduardo, Anthony Ma, and Osama Idrees. CERTS Microgrid Demonstration with Large-scale Energy Storage and Renewables at Santa Rita Jail: Final Project Report. Vol. 1. State of California Energy Commission, 2014.

[29] Johnson, Brian, et al. "A unified dynamic characterization framework for microgrid systems." Electric Power Components and Systems 40.1 (2011): 93-111.

[30] Umar, Muhammad. Modeling and simulation of The CERTS Microgrid: a comparative study using PSCAD and MATLAB SIMSCAPE. University of Ontario Institute of Technology (Canada), Doctoral dissertation) 2020.

[31] Abdelgayed, Tamer S., Walid G. Morsi, and Tarlochan S. Sidhu. "A new approach for fault classification in microgrids using optimal wavelet functions matching pursuit." IEEE Transactions on Smart Grid 9.5 (2017): 4838-4846.

[32] R. H. Lasseter, J. H. Eto, B. Schenkman, J. Stevens, H. Vollkommer, D. Klapp, et al., "CERTS microgrid laboratory test bed," IEEE Trans. Power Del., Jan. 2011, vol. 26, no. 1, pp. 325–332.

[33] Rayane Mourouvin, Juan Carlos Gonzalez-Torres, Jing Dai, Abdelkrim Benchaib, Didier Georges, et al. Understanding the role of VSC control strategies in the limits of power electronics integration in AC grids using modal analysis. Electric Power Systems Research, 2021, 192 (March), pp.106930. 10.1016/j.epsr.2020.106930. hal-03651565.

[34] I. Colak, "Introduction to smart grid," in 2016 International Smart Grid Workshop and Certificate Program (ISGWCP), Istanbul, Turkey, 2016, pp. 1–5, doi: 10.1109/ISGWCP.2016.7548265.

[35] Yazdani, and R. Iravani, Voltage-sourced converters in power systems: modeling, control, and applications. John Wiley & Sons, Mar. 2010.

Online ISSN: 3009-7800
Print ISSN: 3009-6324

[36] Saad, E., Elkoteshy, Y., & AbouZayed, U. (2020). Modeling and analysis of grid-connected solar-PV system through current-mode controlled VSC. In E3S Web of Conferences (Vol. 167, p. 05005). EDP Sciences.
[37] A. Yazdani and P. Dash, "A control methodology and characterization of dynamics for a photovoltaic (PV) system interfaced with a distribution network," IEEE Trans. Power Del., vol. 24, no. 3, pp. 1538– 1555, Jul. 2009.
[38] Liu, Heping, Ping Liu, and YuXin Zhang. "Design and digital implementation of voltage and current mode control for the quasi-Z-source converters." IET Power Electronics 6.5 (2013): 990-998.
[39] Sousa, S. M., et al. "MPPT algorithm in single loop current-mode control applied to dc-dc converters with input current source characteristics." International Journal of Electrical Power & Energy Systems 138 (2022): 107909.
[40] Ellabban, Omar, Joeri Van Mierlo, and Philippe Lataire. "Voltage mode and current mode control for a 30 kW high-performance Z-source Inverter." 2009 IEEE Electrical Power & Energy Conference (EPEC). IEEE, 2009.
[41] Han, Jungho, and Joong-Ho Song. "Phase current-balance control using DC-link current sensor for multiphase converters with discontinuous current mode considered." IEEE Transactions on Industrial Electronics 63.7 (2016): 4020-4030.
[42] Trescases, Olivier, Aleksandar Prodić, and Wai Tung Ng. "Digitally controlled current-mode DC-DC converter IC." IEEE Transactions on Circuits and Systems I: Regular Papers 58.1 (2010): 219-231.
[43] Ghalebani, Pedram, Vahid Teymoori, and Fredrick Mukundi Mwaniki. "Digital peak current mode control of isolated current-fed push-pull DC-DC converter with slope compensation." International Journal of Circuit Theory and Applications 50.3 (2022): 779-793.
[44] Naderi, Seyed Behzad, Michael Negnevitsky, and Kashem M. Muttaqi. "A modified DC chopper for limiting the fault current and controlling the DC-link voltage to enhance fault ride-through capability of the doubly-fed induction-generator-based wind turbine." IEEE Transactions on Industry Applications 55.2 (2018): 2021-2032.
[45] Malik SM, Ai X, Sun Y, Zhengqi C, Shupeng Z. Voltage and frequency control strategies of hybrid AC/DC microgrid: a review. IET Generation, Transmission & Distribution. 2017 Jan;11(2):303-13.

Online ISSN: 3009-7800
Print ISSN: 3009-6324